Electrical properties of polyaniline doped with metal ions

6 authors, including:

Gunadhor Okram
UGC-DAE Consortium for Scientific Research
192 PUBLICATIONS   **1,176** CITATIONS

SEE PROFILE

Ajay Soni
Indian Institute of Technology Mandi
71 PUBLICATIONS   **1,058** CITATIONS

SEE PROFILE

Biswajit Ghosh
Jadavpur University
48 PUBLICATIONS   **1,347** CITATIONS

SEE PROFILE

Some of the authors of this publication are also working on these related projects:

Project   X-ray Photoelectron Spectroscopy View project

Project   CdS-SnS based Solar Cell- M.Tech Project View project

Electrical properties of polyaniline doped with metal ions

J B M Krishna[1,4]**, A Saha**[1]**, G S Okram**[2]**, A Soni**[2]**, S Purakayastha**[3] **and B Ghosh**[3]

[1] UGC-DAE Consortium for Scientific Research, Kolkata-700 098, India
[2] UGC-DAE Consortium for Scientific Research, Indore-452017, India
[3] School of Energy Studies, Jadavpur University, Kolkata-700032, India

E-mail: jbmk@alpha.iuc.res.in

Abstract
Electrical transport properties of undoped polyaniline (Pani) and Pani doped with Fe, Ni and La ions (named Pani–Fe, Pani–Ni and Pani–La) have been investigated using dc and ac conductivity data. It is shown that the Pani–Fe sample follows 3D variable range hopping (VRH) conduction while the Pani, Pani–Ni and Pani–La samples follow 1D VRH conduction. These results are discussed by comparing with conventional HCl-doped Pani. Ac conductivity studies carried out in the frequency range 42 Hz–5 MHz reveal the influence of dopants on inter-chain interactions. The dielectric response exhibits two well resolved relaxation processes, which appear to indicate phase segregation of doped and undoped regions in the samples.

1. Introduction

Polyaniline (Pani) is a very well-known conducting polymer which has attracted a lot of attention due to its promising applications [1] in anticorrosion coatings [2, 3], electrodes in secondary batteries [4], active components in LEDs [5, 6], etc. The ease of synthesis, reasonably high electrical conductivity and good environmental stability make it a potential candidate for use in organic electronic devices [7]. Indeed, Pani is a dynamic block copolymer consisting of reduced benzoid units and oxidized quinoid units [8]. It can exist in several oxidation states, as shown in figure 1, right from fully reduced leucoemeraldine (*a*) to fully oxidized pernigraniline (*b*). Its half oxidized form (*c*) is known as emeraldine base (EB), which is an insulator. Each tetramer of EB consists of two amine and two imine nitrogen atoms. EB can be doped to obtain the conducting Pani. The most popular method of doping Pani is by protonation using inorganic or organic Bronsted acids, in which the imine nitrogens preferentially get protonated [8] and the electrical conductivity varies over a wide range as a function of the pH of the acid used for doping. Doping has also been achieved by using Lewis acids such as $SnCl_4$, $FeCl_3$, $GaCl_3$, $AlCl_3$ and $EuCl_3$ [9–11]. Unlike the protonation by Bronsted acids, Lewis acid doping occurs both on imine and amine nitrogen atoms on the polymer backbone and hence this
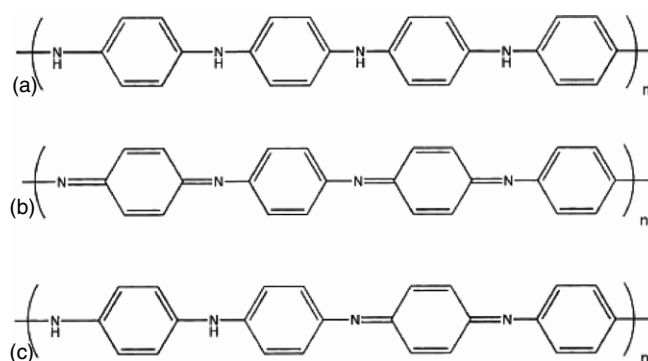

Figure 1. Different oxidation states of Pani. (*a*) Leucoemeraldine, (*b*) pernigraniline, (*c*) EB.

is expected to have a bearing on the solution processability of the polymer [12, 13]. In fact, the metal cations of the inorganic salts form complexes with Pani [14] and the material exhibits different properties depending on the dopant–polymer–solvent interactions [15]. The studies on interaction of the metal ions with Pani suggest that the metal ions oxidize the benzoid group in Pani and the reduced metal ion forms a co-ordination complex with the Pani molecule [16].

Electrical transport studies on cobalt-doped Pani are reported to follow 3D variable range hopping (VRH) [17]. However, the observed lower inter-chain coupling [12, 13]

[4] Author to whom any correspondence should be addressed.

due to doping at imine and amine sites does not correlate with the 3D nature of electrical conduction in Lewis acid doped Pani. Although the observed electrical conductivity is generally explained on the basis of formation of polaron band in the band gap, the details of the interaction between the metal ion and the polymer chain leading to the formation of polaron lattice are still not very well understood. In view of the wide variety of dopants available in the form of Lewis acids, a clear understanding of their interactions with Pani will help in better applications of these materials. In this study we have investigated electrical transport in metal ion doped Pani using the temperature dependent dc electrical conductivity and frequency dependent ac conductivity on conventional HCl-doped Pani (Pani–H), Pani–Fe, Pani–Ni and Pani–La samples. Critical analysis of the data indicates that the Pani–H and Pani–Fe samples follow 3D VRH conduction while the Pani–Ni and Pani–La samples follow 1D VRH conduction.

2. Experimental section

2.1. Sample preparation

Pani was synthesized following a method reported earlier [8]. Briefly, 20 ml of double distilled aniline was dissolved in 300 ml of 1 M HCl and 11.5 g ammonium peroxydisulfate (APS) was dissolved in 200 ml 1 M HCl and both were cooled to ∼1 °C in an ice bath. The APS solution was added to the aniline solution drop-wise with constant stirring over a period of 1 min. The solution was stirred for ∼1.5 h in an ice bath. The solution was filtered by a vacuum filtration and the precipitate was washed with 750 ml of 1 M HCl to remove the unreacted aniline and its oligomers from the precipitate. Pani synthesized by this method is formed in its protonated state and is dark green in colour. The precipitate was dried, weighed and allowed to equilibrate with an appropriate amount of ammonium hydroxide overnight. This process de-doped the Pani to its EB form. The dispersion was filtered and freeze-dried. The sample was ground to a fine powder using a mortar and a pestle. 100 ml aqueous solutions of the dopants $FeCl_3$, $NiCl_2$, $LaCl_3$ and HCl of appropriate concentrations were prepared and 1 g EB powder was added to each of them and kept overnight with constant stirring. The molar ratio of a tetramer unit of EB to dopant was kept 1 : 2 in all the samples. The solutions were filtered, and the precipitate was freeze-dried. Samples were compressed into pellets of 10 mm diameter and 1 mm thickness by applying a pressure of ∼250 kg cm^{-2}.

2.2. X-ray diffraction (XRD) measurements

For studying the structural changes due to incorporation of metal ions in Pani, XRD measurements were carried out. XRD patterns were obtained using Bruker D8/Discover diffractometer with monochromatic Cu K$_a$ x-rays (λ = 1.542 Å) for the samples in the form of pellets.

2.3. Raman spectroscopy measurements

Raman spectroscopy measurements were conducted to identify the chemical species formed due to incorporation of metal ions into the Pani samples. Raman spectroscopy was carried out using a LABRAM-HR (Jobin Yvon Horibra) Raman spectrometer.

2.4. Dc conductivity measurements

Temperature dependent dc conductivity measurements were carried out on the samples in the temperature range from 80 to 300 K. A Lakeshore temperature controller was used to control the sample temperature. The resistivities of the Pani–Fe and Pani–H samples were measured by the standard 4-probe method, while guarded 2-probe measurements were carried out for the undoped Pani, Pani–Ni and Pani–La samples, as their resistances were high. Keithley current source 6221 and electrometer 6517A were used for 4-probe measurements and only a Keithley electrometer 6517A was used in two probe measurements. Electrical contacts were made using highly conducting silver paste.

2.5. Ac conductivity measurements

AC conductivity measurements were carried out using a Tegam 3550 LCR meter. Sample pellets were prepared in capacitor geometry by coating a thin layer of silver paste on both sides and attaching silver leads. Samples were mounted on a test fixture (TEGAM 3510) and capacitance and dissipation factor were measured as a function of frequency in the range from 42 Hz to 5 MHz.

3. Results and discussion

XRD patterns of the undoped, HCl-doped and metal-doped samples are shown in figure 2. As mentioned in section 2.1, the undoped PANI (EB) was obtained after deprotonation of emeraldine hydrochloride formed as a result of the synthesis method used. The undoped Pani obtained by this procedure is known as EB-I [18]. Earlier studies have shown that the XRD pattern for the EB-I form of PANI exhibits characteristics of crystalline as well as amorphous phases in the sample [19]. The crystalline component of the XRD pattern shows Bragg reflections around 15°, 20° and 24° [19]. Based on these studies, the proposed unit cell for EB-I has two PANI chains parallel to the *z*-direction and the observed diffraction peaks have been shown to arise due to reflections from crystalline phases having unit cell structure mentioned above [18, 19]. However, in this study we observe a broad hump, having a maximum around 20° and a shoulder at 24° for the undoped sample, as shown in figure 2(*a*). In the absence of sharp peaks, it might be concluded that the undoped sample in this case consists mostly of the amorphous phase. Doping of EB-I with HCl results in the transformation of the structure to the so-called ES-I form [18, 19]. The dopant molecules attaching to the nitrogen atoms on the polymer backbone might take up the positions in the channels formed by the PANI chains. The diffraction pattern of Pani–H, shown in figure 2(*b*), exhibits sharp peaks when compared with the undoped sample. In this case the most intense peak appears at 25°, which might be related to the ordering of dopant molecules
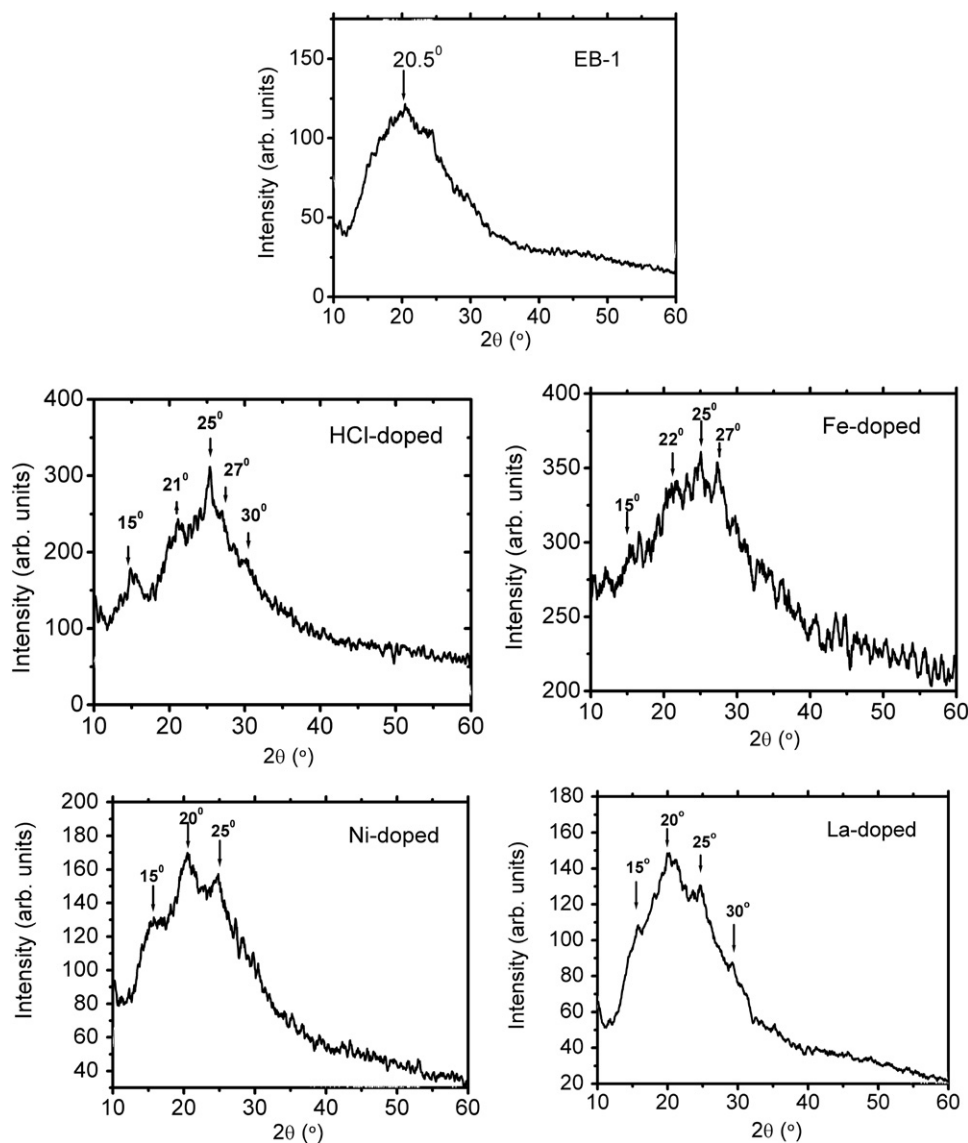
Figure 2. XRD patterns for undoped and doped Pani samples as indicated.

in the channels between the polymer chains [20]. It appears that the incorporation of dopants into the channels between the polymer chains leads to better alignment of the polymer chains. Although the diffraction pattern for Pani–Fe, shown in figure 2(*c*), is noisy, its general trend is similar to that for Pani–H. The XRD pattern for Pani–Ni, shown in figure 2(*d*), exhibits peaks at 20° and 25°. In the case of Pani–La also, the XRD pattern shows peak at 20° and a shoulder at 25° as seen in figure 2(*e*). On comparing the XRD patterns of the doped samples with that of the undoped sample, it can be said that doping has resulted in a relative increase in crystalline phases in the sample. The degree of crystalline ordering seems to be dependent on the size of the dopant as can be qualitatively seen from the fact that the peaks are relatively sharper in Pani–H followed by Pani–Fe, Pani–Ni and Pani–La.

The Raman spectrum taken at an excitation wavelength of 632.8 nm for the samples is shown in figure 3. The spectrum shows peaks, which can be associated with characteristic bands of the quinone and semi-quinone structures in the
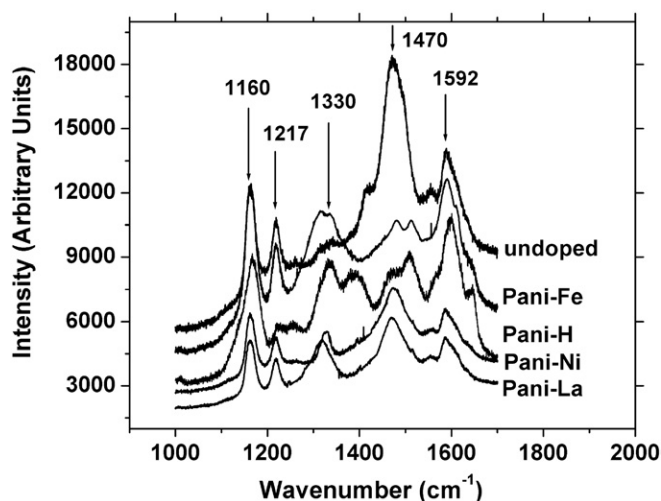

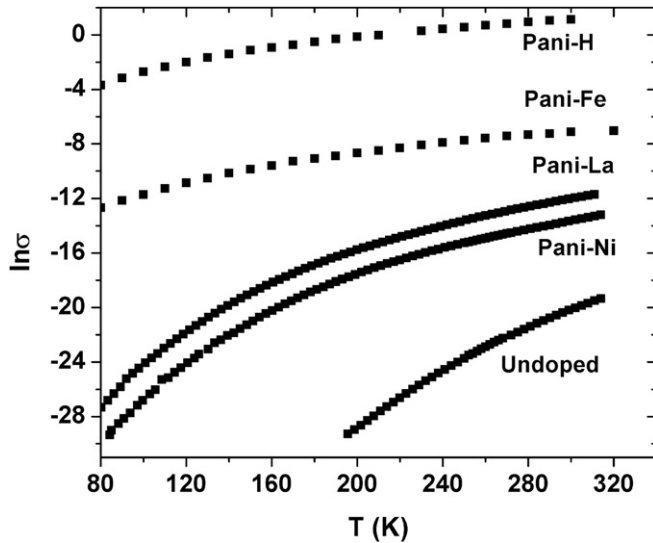**Figure 3.** Raman Spectrum for undoped and doped samples as indicated.

Figure 4. ln σ versus temperature for undoped and doped Pani samples as indicated.

undoped and doped samples, respectively. The band at 1160 cm^{-1} corresponds to the β_{C-H} vibration of the quinoid ring, 1217 cm^{-1} corresponds to ν_{C-N}, 1470 cm^{-1} corresponds to $\nu_{C=N}$ and 1592 cm^{-1} corresponds to $\nu_{C=C}$. All these bands are characteristic of quinone segments [21]. The observed bands agree with the known chemical structure of EB. For all the metal-doped samples, there is a decrease in the intensity of the band at 1470 cm^{-1}, corresponding to quinone segments, when compared with EB. A new band associated with ν_{C-N+} appears around 1330 cm^{-1}, corresponding to semi-quinone segments [22]. The decrease in the intensity for quinone bands and the appearance of bands corresponding to semi-quinone segments indicates the doping of EB with metal ions. The bands at 1162 cm^{-1} (ν_{C-H}) and 1219 cm^{-1} (ν_{C-N}) are assigned to reduced amine benzene ring.

The variation of dc conductivity with temperature for all the samples is shown in figure 4. It is interesting to note that the conductivity in the Pani–Ni and Pani–La samples is several orders of magnitude lower than those of the Pani–H and Pani–Fe samples. The higher dc electrical conductivity observed for the Pani–H and Pani–Fe samples might be due to better inter-chain overlap between the Pani chains in these samples. To investigate the electrical transport critically in these conducting polymers, we applied the well-known Mott's VRH theory [23], according to which the conductivity

$$\sigma = \sigma_0 \left(-\frac{T_0}{T} \right)^{\gamma}, \tag{1}$$

where $\gamma = 1/(d+1)$, d being the dimensionality of the hopping process. For 3D VRH $\gamma = 1/4$, for 2D VRH $\gamma = 1/3$ and for 1D VRH $\gamma = 1/2$. T_0 is a characteristic temperature related to the activation energy required for hopping given by [24]

$$T_0 = \frac{16\alpha^3}{k_B N(E_F)}, \tag{2}$$

where α is the inverse of the localization length and $N(E_F)$ is the density of states at Fermi level. The dimensionality

of the conduction process and T_0 can be determined by fitting equation (1) with the measured data. T_0 is related to the average hopping distance according to the relation [24]

$$R_{\text{hop}} = \left[\frac{9}{8\pi\alpha k_B T N(E_F)} \right]^{1/4}. \tag{3}$$

The value of R_{hop} can be used to estimate the average hopping energy, W [24]:

$$W = \frac{3}{4\pi R_{\text{hop}}^3 N(E_F)}. \tag{4}$$

The dc conductivity data ware analysed by applying 1D, 2D and 3D VRH models for all the samples. The linear fits to the ln σ versus $T^{-\gamma}$ plots are shown in figures 5–7. As can be seen from figures 5(a)–(d), the data for the Pani–H and Pani–Fe sample does not fit the 1D and 2D VRH models. Similarly, figures 5(e)–(h) show that the data for Pani–Ni and Pani–La do not fit the 2D and 3D VRH models. Based on the least square fitting, the best fit obtained for the Pani–H and Pani–Fe samples is shown in figure 6. As can be seen from figure 6, the conductivity in the Pani–H and Pani–Fe samples follows 3D VRH. Similarly for the undoped Pani, Pani–Ni and Pani–La samples, the best fit is obtained with the 1D-VRH model, as shown in figure 7. It is therefore clear that conductivity in all the samples follows Mott's VRH. This is clear from the fit of equation (1) to the measured conductivity data of the samples, keeping T_0 and γ as free parameters. The value of T_0 is obtained from the slope of the best fit plots for all the samples.

Using a typical value of three states per electronvolt per two rings for the density of states at Fermi level [17] the calculated values of localization length α^{-1}, average hopping distance R_{hop} and average hopping energy W_{hop} are given in table 1. The localization length in Pani–H and Pani–Fe are significantly larger than those of undoped Pani, Pani–H and Pani–La. A similar trend is followed in the average hopping distance. Conversely, the hopping energy is smaller in the former two samples compared with the latter three samples. Thus, these parameters clearly explain the electrical transport properties in these conducting polymers. The 3D VRH observed in the Pani–Fe and Pani–H samples suggests that the dopants in these samples provide better pathways between neighbouring chains resulting in a 3D conducting network. The 1D nature observed in the undoped Pani, Pani–Ni and Pani–La samples shows that the motion of the charge carriers is restricted mostly to a single chain or at the most to the nearest neighbours.

The capacitance (C) and the dissipation factor (D) of the samples were measured as a function of frequency (f) of the applied voltage. The dissipation factor in the Pani–Fe and Pani–H samples was very high at low frequencies due to the high conductivity of these samples, and was beyond the range of the LCR meter. The real and imaginary components of the dielectric constant were calculated from the following relations

$$\varepsilon' = \frac{Cd}{\varepsilon_0 A}, \tag{5}$$
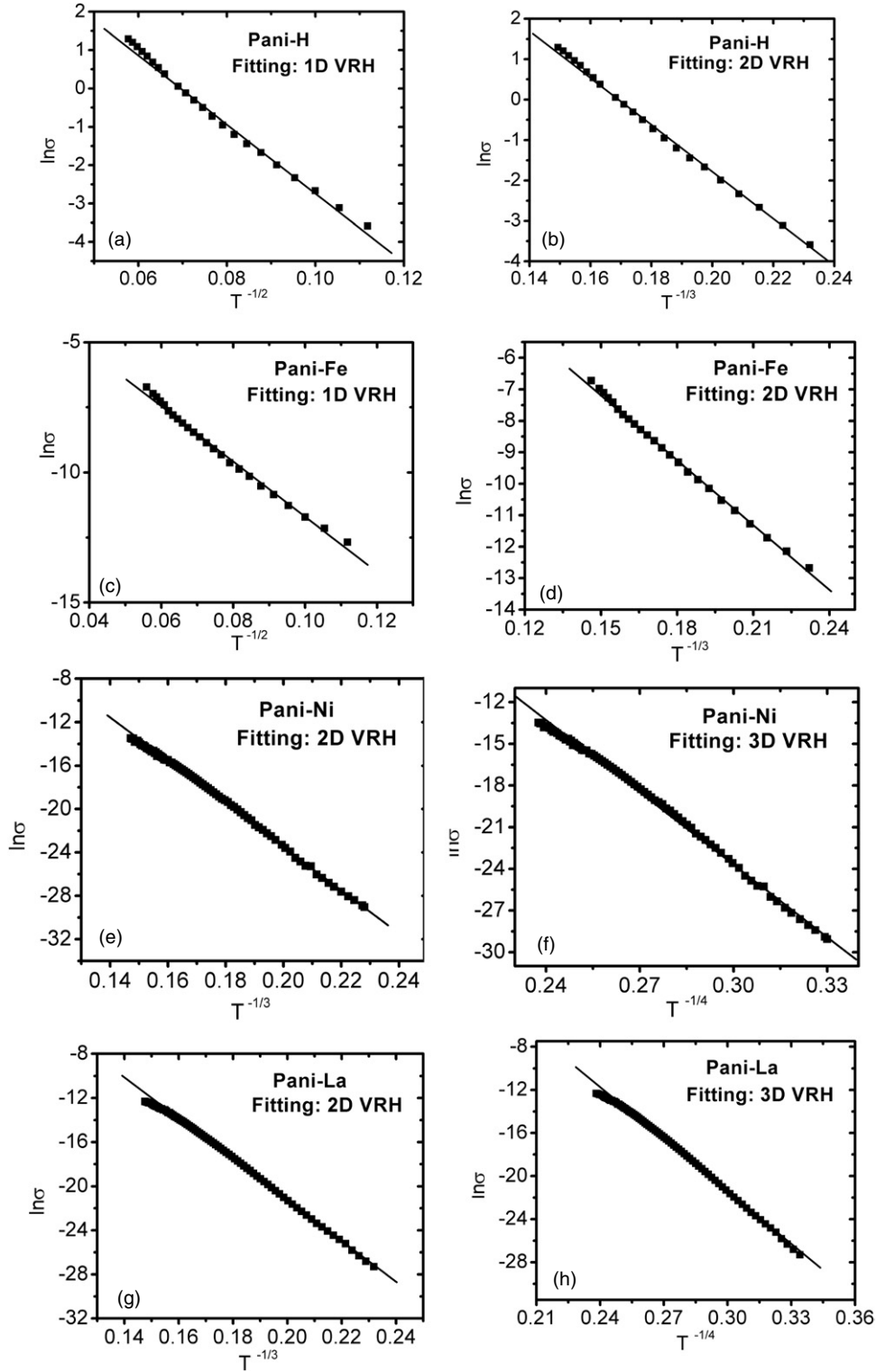
$$\varepsilon'' = \varepsilon' D, \tag{6}$$

Figure 5. Fitting of dc conductivity data to VRH models (*a*) 1D VRH model applied to Pani–H, (*b*) 2D VRH applied to Pani–H, (*c*) 1D VRH applied to Pani–Fe, (*d*) 2D VRH applied to Pani–Fe, (*e*) 2D VRH applied to Pani–Ni, (*f*) 3D VRH applied to Pani–Ni, (*g*) 2D VRH applied to Pani–La, (*h*) 3D VRH applied to Pani–La.

where ε_0 is the permittivity of free space ($= 8.85 \times 10^{-12}\,\mathrm{F\,m^{-1}}$), A is the area of the electrodes and d is the sample thickness. In disordered materials like Pani, hopping of the charge carrier (polaron) to a new site in response to the applied field leads to successful charge transport only if the polarization cloud around the charge also follows it. The

mutual movement of the charge and the associated polarization cloud requires an electric relaxation time τ. The relaxation time can be calculated from the frequency at which the ε''–f plot peaks [25].

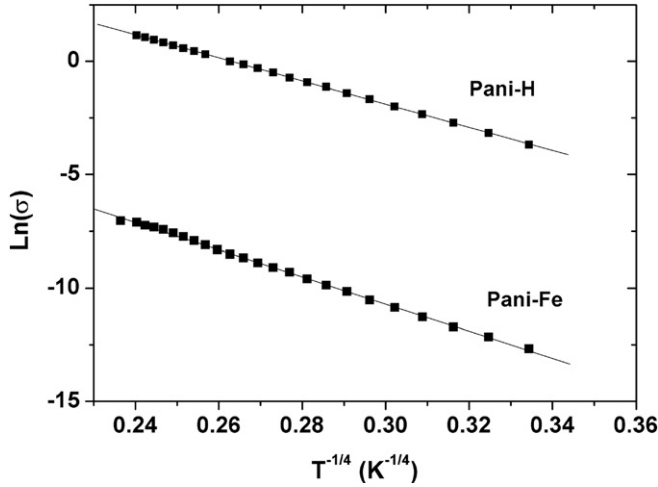The variation of the imaginary component of the dielectric constant with frequency is shown in figure 8. As can be seen,

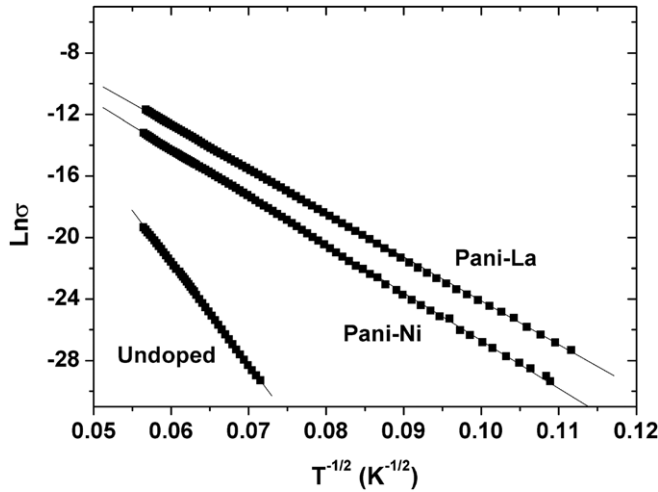**Figure 6.** $\ln \sigma$ versus $T^{-1/4}$ for Pani–Fe and Pani–H samples.

Figure 7. $\ln \sigma$ versus $T^{-1/2}$ for undoped Pani, Pani–Ni and Pani–La samples.

Table 1. Parameters extracted from the dc conductivity versus temperature data.

Sample	α^{-1} (Å)	R_{hop} (Å)	W_{hop} (eV)
Pure Pani	5.3	12.7	0.041
Pani–H	26	19.0	0.012
Pani–Fe	18	17.3	0.016
Pani–Ni	9.3	14.7	0.028
Pani–La	8.8	14.5	0.027

the ε'' versus f plot does not show any peak in the measured frequency region. This may be due to the high conductivity and/or electrode polarization effects in the samples, which mask the relaxation processes [25]. In such cases electric modulus formalism is used [25, 26], which eliminates the electrode effects. Electric modulus (M) is defined as
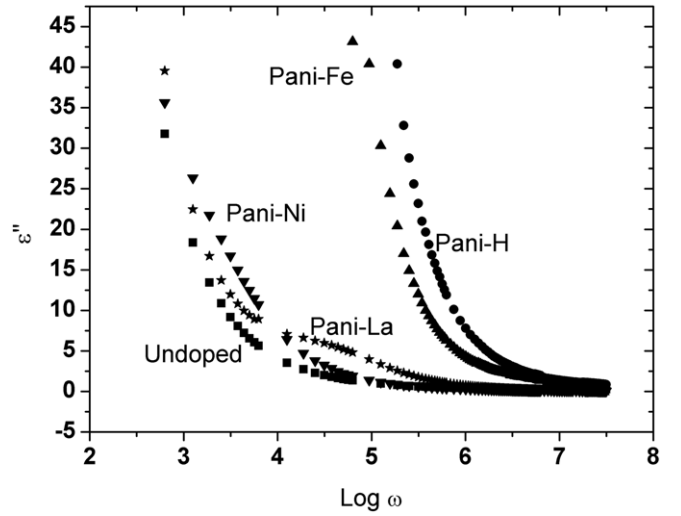
$$M^* = \frac{1}{\varepsilon^*}. \qquad (7)$$

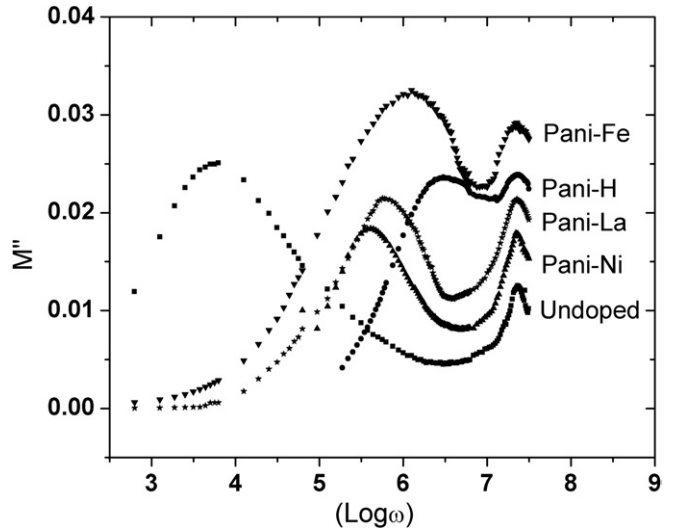**Figure 8.** ε'' versus f for undoped and doped samples as indicated.

Figure 9. M'' versus f for undoped and doped samples as indicated.

The real and imaginary parts of M are given by

$$M' = \frac{\varepsilon'}{(\varepsilon')^2 + (\varepsilon'')^2}, \qquad (8)$$

$$M'' = \frac{\varepsilon''}{(\varepsilon')^2 + (\varepsilon'')^2}. \qquad (9)$$

The relaxation time can also be determined from the peak in the M''–f plot. Variation of M'' with frequency is shown in figure 9.

M'' versus $\mathrm{Log}(\omega)$ plots show two distinct peaks for all the samples. The peak at high frequency is at the same position for the pure as well as the doped samples. This peak could be associated with intra-chain hopping of charge carriers in the undoped regions of the samples. Since all the samples have the same polymer backbone one would expect that the relaxation time for on-chain transport is comparable for all the samples. However the position of the peak at the lower frequency appears to depend on the dopant. This might be associated with inter-chain hopping of charge carriers through the doped regions on the polymer chain. For the Pani–H and

Pani–Fe samples this peak is at a higher frequency, which corresponds to a lower relaxation time compared with that in the Pani–Ni and Pani–La samples. From the ac conductivity measurements it appears that inter-chain hopping of charge carriers in the Pani–H and Pani–Fe samples is easier than that in the Pani–Ni and Pani–La samples. This is also consistent with the higher conductivities observed and 3D VRH found in the Pani–H and Pani–Fe samples. It may be noted that the same peak for the undoped sample is at a much lower frequency, i.e. higher relaxation time, indicating that inter-chain charge hopping is much more difficult in the absence of dopants.

4. Conclusions

Metal ion doped Pani samples were synthesized chemically and charge transport in these samples was studied. Dopants seem to have a strong influence on the charge transport. Dc conductivity studies show that the dopants in the Pani–H and Pani–Fe samples interact strongly with Pani chains and form 3D conducting networks. The 3D hopping nature and higher values of dc conductivities in these samples are consistent with higher inter-chain carrier mobility observed in ac conductivity studies. Though the doping concentrations in the Pani–Ni and Pani–La samples were identical to that of the Pani–H and Pani–Fe samples, their conductivities are significantly low. Ac conductivity studies show that lower conductivity is mainly due to the lower inter-chain carrier mobility.

Acknowledgments

References

[1] Kang E T, Neoh K G and Tan K L 1998 *Prog. Polym. Sci.* **23** 277

[2] Wessling B 1994 *Adv. Mater.* **6** 226

[3] Lu W K, Elsenbaumer R L and Wessling B 1995 *Synth. Met.* **71** 2163

[4] MacDiarmid A G, Yang L S, Huang W S and Humphrey B D 1987 *Synth. Met.* **18** 393

[5] Wang H L, MacDiarmid A G, Wang Y Z, Gebler D D and Epstein A J 1996 *Synth. Met.* **78** 33

[6] Chen S A, Chung K R, Chao C L and Lee H T 1996 *Synth. Met.* **82** 207

[7] Neoh, K G, Kang E T, Khor S H and Tan K L 1990 *Polym. Degrad. Stab.* **27** 107

[8] Shimano J Y and MacDiarmid A G 2001 *Synth. Met.* **121** 251

[9] Dimitrev O P and Kislyuk V V 2002 *Synth. Met.* **132** 87

[10] Bienkowski K, Bajer I K, Genoud F, Oddou J L and Pron A 2003 *Synth. Met.* **135–136** 159

[11] Dimitrev O P 2004 *Synth. Met.* **142** 299

[12] Yang C and Chen C 2005 *Synth. Met.* **153** 133

[13] Kulsewich-Bajer I, Pron A, Abramowicz J, Jeandey C, Oddou J L and Sobczak J W 1999 *Chem. Mater.* **11** 552

[14] Genoud F, Kulsewich-Bajer I, Bedel A, Oddou J L, Jeandey C and Pron A 2000 *Chem. Mater.* **12** 744

[15] Celly-Izumi M S, Ferreira Anna Maria C, Constantino Vera R L and Temperini Marcia L A 2007 *Macromolecules* **40** 3204

[16] Dimitrev O P, Smertenko P S, Stiller B and Brehmer L 2005 *Synth. Met.* **149** 187

[17] Ghosh P, Sarkar A, Meikap A K, Chattopadhyay S K, Chatterjee S K and Ghosh M 2006 *J. Phys. D: Appl. Phys.* **39** 3047

[18] Pouget J P, Jozefowicz M E, Epstein A J, Tang X and MacDiarmid A G 1991 *Macromolecules* **24** 779

[19] Luzny W, Sniechowski M and Laska J 2002 *Synth. Met.* **126** 27

[20] Uny W and Baka E 2000 *Macromolecules* **33** 425

[21] Quillard S, Louam G, Lefrant S and MacDiarmid A G 1994 *Phys. Rev.* B **50** 12496

[22] Celly-Izumi M S, Constantino Vera R L, Ferreira Anna Maria C and Temperini Marcia L A 2000 *Synth. Met.* **156** 654

[23] Mott N F and Davis E A 1979 *Electronic Processes in Non Crystalline Materials* 2nd edn (Oxford: Clarendon)

[24] Campos M and Bello B Jr 2006 *J. Phys. D: Appl. Phys.* **30** 1531

[25] Singh R, Arora V, Tandon R P, Mansingh A and Chandra S 1999 *Synth. Met.* **104** 137

[26] Calleja R D, Matveeva E S and Parkhutik V P 1995 *J. Non-Cryst. Solids* **180** 260